utilizing n-GaAs electrodes in $AlCl_3$–BPC molten salts and the good stability demonstrated by these electrodes in the 1:1 electrolyte are encouraging. The results described above also suggest that considerable scope exists in the use of molten salts as electrolytes in photoelectrochemical systems.

Acknowledgments. The authors express their appreciation to the Solar Energy Research Institute and the U.S. Department of Energy for financial support of this research program. Thanks are also due to R. J. Gale for stimulating discussions on molten-salt electrolytes.

The High-Spin ($^5T_2$) ⇌ Low-Spin ($^1A_1$) Transition in Solid Bis(1,10-phenanthroline-2-carbaldehyde phenylhydrazone)iron(II) Diperchlorate. Simultaneous Change of Molecular Spin State and Crystallographic Structure

E. König,*[1a] G. Ritter,[1b] W. Irler,[1b] and H. A. Goodwin[2]

Contribution from the Institut für Physikalische und Theoretische Chemie and Physikalisches Institut, Abt. II, University of Erlangen-Nürnberg, D-8520 Erlangen, West Germany, and the School of Chemistry, The University of New South Wales, Kensington, N.S.W. 2033, Australia.
Received October 22, 1979

Abstract: The six-coordinate iron(II) complex $[Fe(phy)_2](ClO_4)_2$ (phy = 1,10-phenanthroline-2-carbaldehyde phenylhydrazone) has been shown by variable-temperature ^{57}Fe Mössbauer effect, X-ray diffraction, and magnetic measurements to exhibit a high-spin ($S = 2$; $^5T_2$) ⇌ low-spin ($S = 0$; $^1A_1$) transition in the solid state. The ground states involved are characterized, at the transition temperature T_c, by $\Delta E_Q(^5T_2) = 0.91$ mm s^{-1}, $\delta^{IS}(^5T_2) = +0.93$ mm s^{-1} and $\Delta E_Q(^1A_1) = 1.61$ mm s^{-1}, $\delta^{IS}(^1A_1) = +0.28$ mm s^{-1}. For sample I of $[Fe(phy)_2](ClO_4)_2$, a pronounced hysteresis of $\Delta T_c = 8.1$ K has been observed, the transition being centered at $T_c\uparrow = 256.1$ K for rising and at $T_c\downarrow = 248.0$ K for lowering of temperature. The Debye–Waller factors at $T_c\uparrow$ ($f_{^5T_2} = 0.116$, $f_{^1A_1} = 0.198$) show a discontinuity of $\Delta f_{total} \approx 42\%$, the temperature function of both $f_{^5T_2}$ and $f_{^1A_1}$ being well reproduced within the high-temperature approximation of the Debye model ($\Theta_{^5T_2} = 127.3$ K, $\Theta_{^1A_1} = 146.8$ K, $M_{Fe} = 57$ au). The X-ray diffraction patterns for the $^5T_2$ and $^1A_1$ phases are characteristically different. The temperature dependence of the molecular fraction $n_{^5T_2}$, including details of the hysteresis curve, is the same whether determined from the Mössbauer data or the X-ray peak profiles. Thus a concomitant change in the electronic state of the molecules and crystallographic properties of the lattice occurs at T_c. The $^5T_2 \rightleftharpoons {}^1A_1$ transition is thermodynamically first order. The observed equal areas of scanning curves are indicative, within the Everett model, of the formation of independent domains by both $^5T_2$ and $^1A_1$ molecules. From the line widths of X-ray diffraction patterns, the magnitude of the domains follows as ≥5000 Å. In a second sample, sample II of $[Fe(phy)_2](ClO_4)_2$, the first-order character of the $^5T_2 \rightleftharpoons {}^1A_1$ transition is diminished presumably due to impurities and/or defects in the solid. After recrystallization, sample II gives results similar to those of sample I.

Introduction

Temperature- or pressure-induced transitions between two states of differing spin multiplicity have been observed in certain complexes of d^5, d^6, d^7, and d^8 ions of the first-transition series.[3-5] The high-spin ($^5T_2$) ⇌ low-spin ($^1A_1$) transition which is characteristic for the (approximately octahedral) six-coordinated d^6 configuration has been also encountered in certain perovskites like $LaCoO_3$[6] and in mixed sulfides of the type $Fe_xTa_{1-x}S_2$.[7] Moreover, the variable spin state of iron proteins is believed to be of importance for the catalytic properties of these bioactive systems.[8] In solution, the spin interconversion process is dynamic in nature, and its mechanism seems to be reasonably well understood.[9,10] Thus rate constants for the process

$$\text{low spin} \underset{k_{-1}}{\overset{k_1}{\rightleftharpoons}} \text{high spin}$$

have been determined for a number of spin-interconversion systems and for iron(II) complexes; for example, the values obtained for k_1 and k_{-1} vary between 4×10^5 and 2×10^7 s^{-1}.[11]

The first example of a high-spin ($^5T_2$) ⇌ low-spin ($^1A_1$) transition was established for a solid complex,[12] and most subsequent studies have been concerned with systems in the solid state. Recent progress with spin transitions in the solid state has, however, been slow due to unpredictable lattice effects arising from variable degrees of solvation, different crystal forms of the same complex, or perhaps even the influence of slight differences in the

(1) (a) Institut für Physikalische und Theoretische Chemie, University of Erlangen-Nürnberg. (b) Physikalisches Institut, Abt. II, University of Erlangen-Nürnberg.
(2) School of Chemistry, University of New South Wales.
(3) R. L. Martin and A. H. White, *Transition Met. Chem.*, **4**, 113 (1968).
(4) E. König, *Ber. Bunsenges. Phys. Chem.*, **76**, 975 (1972).
(5) H. A. Goodwin, *Coord. Chem. Rev.*, **18**, 293 (1976).
(6) V. G. Bhide, D. S. Rajona, G. Rama Rao, and C. N. R. Rao, *Phys. Rev. B*, **6**, 1021 (1972).
(7) M. Eibschütz, M. E. Lines, and F. J. Di Saloo, *Phys. Rev. B*, **15**, 103 (1977).
(8) E. V. Dose, M. F. Tweedle, and L. J. Wilson, *J. Am. Chem. Soc.*, **99**, 3886 (1977).
(9) J. K. Beattie, R. A. Binstead, and R. J. West, *J. Am. Chem. Soc.*, **100**, 3044 (1978).
(10) R. A. Binstead, J. K. Beattie, E. V. Dose, M. F. Tweedle, and L. J. Wilson, *J. Am. Chem. Soc.*, **100**, 5609 (1978).
(11) E. V. Dose, M. A. Hoselton, N. Sutin, M. F. Tweedle, and L. J. Wilson, *J. Am. Chem. Soc.*, **100**, 1141 (1978).
(12) E. König and K. Madeja, *Inorg. Chem.*, **6**, 48 (1967).

0002-7863/80/1502-4681$01.00/0

preparation of the samples. Very detailed physical measurements on carefully prepared substances are required in order to gain understanding of the underlying phenomena. We have shown recently[13] that the investigation of hysteresis effects associated with almost discontinuous high-spin ($^5T_2$) ⇌ low-spin ($^1A_1$) transitions may be useful for the understanding of the mechanism of spin transitions in solids. Additional information may be obtained from the application of multichannel analyzer techniques to the analysis of peak profiles of X-ray diffraction.[14]

In this paper we report the detailed study of hysteresis effects at the high-spin ($^5T_2$) ⇌ low-spin ($^1A_1$) transition in solid $[Fe(phy)_2](ClO_4)_2$ where phy = 1,10-phenanthroline-2-carbaldehyde phenylhydrazone. Whereas the temperature dependence of magnetic properties and the ^{57}Fe Mössbauer effect are employed to follow changes of the molecular electronic ground state, the study of peak profiles of the X-ray diffraction as a function of temperature provides insight into changes of the crystallographic structure. The latter results are of particular significance since to date there are only a few single-crystal X-ray structure studies on spin-transitions available, particularly as far as iron(II) compounds are concerned.[15,16] In addition, all studies of this kind have been limited to two temperatures and therefore cannot furnish a description of the effect, on the structure, of progressive changes in temperature.

Experimental Section

Materials. The phenylhydrazone was prepared directly by interaction of 1,10-phenanthroline-2-carbaldehyde with phenylhydrazine in ethanol. The complex $[Fe(phy)_2](ClO_4)_2$ was obtained by treatment of iron(II) perchlorate with the phenylhydrazone and thus closely followed the preparation of the corresponding fluoroborate.[17] All samples gave satisfactory analyses for C, H, N, and Fe.

Methods. Magnetism was measured by the Gouy method by employing a Newport Instruments variable-temperature balance. Magnetic susceptibilities were corrected for diamagnetism ($\chi_m^{dia} = -371 \times 10^{-6}$ cgs mol^{-1}) and effective magnetic moments were obtained according to $\mu_{eff} = 2.828(\chi_m^{corr}T)^{1/2}$, χ_m^{corr} being the corrected molar magnetic susceptibility and T the temperature in K.

^{57}Fe Mössbauer spectra were measured with a spectrometer of the constant acceleration type (Elscint AME-30A) operating in the multiscaler mode. A 50-mCi source of ^{57}Co in rhodium was used, the calibration being effected with a metallic iron absorber. All velocity scales and isomer shifts are referred to the iron standard at 298 K. To convert to the sodium nitroprusside scale, add +0.257 mm s^{-1}. Movement of the source toward the absorber corresponds to positive velocities. Variable-temperature measurements were performed by using a specially designed superinsulated cryostat, a small heating coil, and liquid nitrogen as coolant. The temperature was monitored by means of a calibrated iron vs. constantan thermocouple and a cryogenic temperature controller (Artronix Model 5301-E). The relative accuracy of temperature was about 0.05 K and the absolute accuracy about ±0.5 K. All measurements were effected with the identical geometrical arrangement for source, absorber, and detector. The resulting data were carefully corrected for nonresonant background of the γ rays, and the individual areas $A(^5T_2)$ and $A(^1A_1)$ were extracted by a computer-based decomposition into Lorentzians.

The following procedure was adopted for the determination of Debye–Waller factors for the $^5T_2$ and $^1A_1$ ground states, $f_{^5T_2}$ and $f_{^1A_1}$, respectively. For an absorber of finite thickness, the normalized area[19] for the ith Mössbauer line is determined by eq 1 (area method[18,19]). In eq

$$A_i = \tfrac{1}{2}\pi f_S \Gamma_0 L(t_i) \tag{1}$$

1, f_S is the Debye–Waller factor of the source, Γ_i the line width of the absorber (in the present case $\Gamma_i = \Gamma_0$ always held where Γ_0 is the natural line width), and $L(t_i)$ the saturation function. The inverse to $L(t_i)$ is required in order to obtain, from the quantity A_i of eq 1, the effective thickness t_i. For $0 \le t_i \le 2$ this function is given in numerical form by eq 2 with an accuracy greater than 1%.

$$t_i(L) = L(t_i)/[1 - \tfrac{1}{4}L(t_i)] \tag{2}$$

Provided that the high-temperature approximation for the Debye–Waller factor is followed by both $f_{^5T_2}$ and $f_{^1A_1}$, i.e., eq 3, where, in particular for the Debye model, $H = C/\Theta_{^5T_2}^2$, L = $C/\Theta_{^1A_1}^2$, and $C = 3E_0^2/Mc^2k$, the effective thickness for the two phases may be written as eq 4. Equation 4 applies for each single line of the quadrupole doublet

$$-\ln f_{^5T_2} = HT$$

$$-\ln f_{^1A_1} = LT \tag{3}$$

$$t_{^5T_2} = dn_{^5T_2}f_{^5T_2} = dn_{^5T_2}e^{-HT} \tag{4}$$

$$t_{^1A_1} = d(1 - n_{^5T_2})f_{^1A_1} = d(1 - n_{^5T_2})e^{-LT}$$

and $d = \tfrac{1}{2}N\beta\delta\sigma_0$, where N is the number of iron atoms per unit volume, β the isotopic abundance, δ the absorber thickness, and σ_0 the resonance cross section. Also, in eq 3, E_0 is the γ-ray energy and M the mass of the absorbing atom. From eq 4 it follows for each individual Mössbauer spectrum measured at the temperature T_k that

$$H_k = -\frac{1}{T_k}[\ln (t_{^5T_2}{}^k + t_{^1A_1}{}^k e^{-(H-L)T_k}) - \ln d] \tag{5}$$

$$L_k = -\frac{1}{T_k}[\ln (t_{^1A_1}{}^k + t_{^5T_2}{}^k e^{-(H-L)T_k}) - \ln d]$$

Here, $\bar{H} = \tfrac{1}{n}\sum H_k$ is the average for n measurements and similarly $\bar{L}$. Equation 5 may be solved by iteration on condition that $\sum(\bar{H} - H_k)^2 =$ min or $\sum(\bar{L} - L_k)^2 =$ min. The resulting values of $\bar{H}$ and $\bar{L}$ determine the Debye–Waller factors of eq 3 and, via eq 4, the $^5T_2$ fraction $n_{^5T_2}$ as well, all three quantities as a function of temperature.

Measurements of X-ray powder diffraction were performed with a Siemens counter diffractometer equipped with an Oxford Instruments CF 108A flow-cryostat. Cu Kα radiation was used. Measurements of peak profiles were carried out in the mode of step scanning of the apparatus, the smallest steps being 0.005° in 2Θ. The resulting pulses were stored and processed by a multichannel analyzer (Elscint MEDA 10), whereas peak areas were determined by summation of background-corrected counting rates. Temperatures were measured by a calibrated resistance thermometer, the relative accuracy of listed temperatures being about 0.1 K, whereas the absolute accuracy is about ±3.0 K. It should be noted that any discrepancy between temperatures quoted for Mössbauer effect and X-ray diffraction measurements is due to the use of different temperature-control equipment for the two techniques.

The relative intensity for a single diffraction line may be written as eq 6. Here, $K(\theta)$ is an angular function comprising the Lorentz, polarization, geometrical and absorption factors, whereas D is the X-ray Debye–Waller factor and $|F|^2$ the structure factor. In the present study, only corresponding closely spaced diffraction lines ($\Delta\theta = 0.4°$ at maximum) at low values of θ are considered. Therefore, the angular function $K(\theta)$ and the Debye–Waller factor D may be taken as practically identical for the two phases, $^5T_2$ and $^1A_1$, cf. eq 6. Moreover, the close position of corresponding diffraction lines for the $^5T_2$ and $^1A_1$ phases suggests that the unit cells for the two phases should not be significantly different. Since it is the same atoms which contribute to the diffraction in both phases, even the structure factors may be assumed to be approximately equal, $|F_{hkl}{}^{^5T_2}|^2 \approx |F_{hkl}{}^{^1A_1}|^2$. In the present circumstances therefore

$$I_{rel} = K(\theta)D\left[n_{^5T_2}\left(F_{hkl}{}^{^5T_2}\right)^2 + (1 - n_{^5T_2})\left(F_{hkl}{}^{^1A_1}\right)^2\right] \tag{6}$$

$$n_{^5T_2} \approx I(^5T_2)/(I(^5T_2) + I(^1A_1)) \tag{7}$$

and $n_{^5T_2}$ determined in this way may be compared with $n_{^5T_2}$ obtained on the basis of Mössbauer effect data.

Results

Sample I. Two independently prepared samples of $[Fe(phy)_2](ClO_4)_2$ have been investigated in full detail, and these will be considered separately in the following. Sample I, in particular, has been obtained by using iron in natural abundance.

The ^{57}Fe Mössbauer effect of $[Fe(phy)_2](ClO_4)_2$, sample I, has been studied between 4.2 and 300 K. Figure 1 shows three typical spectra, i.e., at 251, 257, and 261 K. The spectrum at 251 K is

(13) E. König, G. Ritter, W. Irler, and S. M. Nelson, *Inorg. Chim. Acta*, **37**, 169 (1979).
(14) W. Irler, G. Ritter, E. König, H. A. Goodwin, and S. M. Nelson, *Solid State Commun.*, **29**, 39 (1979).
(15) E. König and K. J. Watson, *Chem. Phys. Lett.*, **6**, 457 (1970).
(16) M. A. Hoselton, L. J. Wilson, and R. S. Drago, *J. Am. Chem. Soc.*, **97**, 1722 (1975).
(17) H. A. Goodwin and D. W. Mather, *Aust. J. Chem.*, **27**, 965 (1974).
(18) G. A. Bykov and Pham Zuy Hien, *Zh. Eksp. Teor. Fiz.*, **43**, 909 (1962).
(19) G. Lang, *Nucl. Instrum. Methods*, **24**, 425 (1963).

Table I. ^{57}Fe Mössbauer Effect Parameters of [Fe(phy)$_2$](ClO$_4$)$_2$ (Sample I) for a Set of Representative Temperatures[a]

T, K	$\Delta E_Q(^1A_1)$,[b] mm s^{-1}	$\delta^{IS}(^1A_1)$,[c] mm s^{-1}	$\Delta E_Q(^5T_2)$,[b] mm s^{-1}	$\delta^{IS}(^5T_2)$,[c] mm s^{-1}	$n_{^5T_2}$
251.0	1.61	+0.28	...	...	0
253.0	1.61	+0.28	0.90 ± 0.02	+0.91 ± 0.03	0.107
256.1	1.61	+0.28	0.91	+0.93	0.505
257.0	1.61	+0.28	0.89	+0.93	0.731
261.0	...	...	0.87	+0.94	1.000
252.8	...	...	0.90	+0.94	1.000
251.0	1.62 ± 0.02	+0.27 ± 0.02	0.90	+0.94	0.940
248.5	1.61	+0.28	0.90	+0.93	0.649
246.0	1.61	+0.28	0.93	+0.91	0.170
243.0	1.61	+0.28	...	...	0

[a] The data are listed in the order of measurement. [b] Experimental uncertainty ±0.01 mm s^{-1} except where stated. [c] Isomer shifts δ^{IS} are listed relative to natural iron at 298 K. Experimental uncertainty ±0.01 mm s^{-1} except where stated.

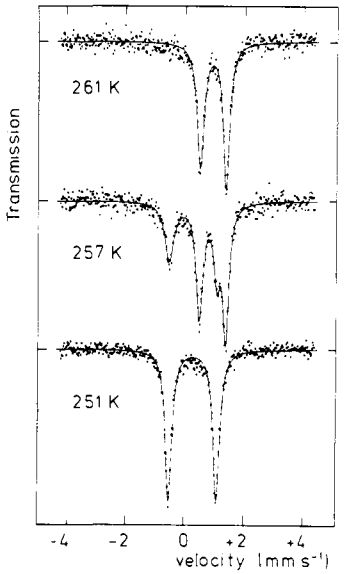

Figure 1. ^{57}Fe Mössbauer effect spectra of [Fe(phy)$_2$](ClO$_4$)$_2$ (sample I) at 251, 257, and 261 K. The measurements were performed for increasing temperatures ($T_c\uparrow$ = 256.1 K).

characterized by the quadrupole splitting ΔE_Q = 1.61 ± 0.01 mm s^{-1} and the isomer shift δ^{IS} = +0.28 ± 0.01 mm s^{-1}. At about 253 K a second weak doublet becomes visible. If the temperature is increased further, the second doublet gains intensity, the first doublet simultaneously decreasing in intensity, cf., e.g., Figure 1, spectrum at 257 K. At 261 K, only the second spectrum is being observed and ΔE_Q = 0.87 ± 0.01 mm s^{-1}, δ^{IS} = +0.94 ± 0.01 mm s^{-1}. The Mössbauer spectra at and above 261 K are practically identical, as are those at and below 251 K. Mössbauer parameters for a number of representative temperatures are listed in Table I. The isomer shift of the 251 K spectrum is characteristic for a low-spin $^1A_1$ spectrum of iron(II) and that of the 261 K spectrum for a high-spin $^5T_2$ ground state. It is thus demonstrated that [Fe(phy)$_2$](ClO$_4$)$_2$ (sample I) shows a high-spin ($^5T_2$) ⇌ low-spin ($^1A_1$) transition between 251 and 261 K. If, starting at, say, 300 K, the temperature is decreased, the $^5T_2$ spectrum changes over into the $^1A_1$ spectrum at a lower temperature than is observed for the $^1A_1 \rightarrow {}^5T_2$ transformation when the sample is heated from below 251 K, thus indicating that hysteresis effects are significant in this system. It should be noted that, in contrast to numerous other iron(II) compounds which undergo a high-spin ($^5T_2$) ⇌ low-spin ($^1A_1$) transition, the values of the quadrupole splitting in both spectra of [Fe(phy)$_2$](ClO$_4$)$_2$ are not typical for the ground state concerned.

In order to demonstrate the hysteresis associated with the transition we have plotted the high-spin fraction $n_{^5T_2}$, as determined from the Mössbauer spectra, in Figure 2 as a function of temperature. The temperature has been gradually increased from 241.0 K to 263.0 K as indicated by the rising arrow. If, subsequently, the temperature is lowered gradually, as indicated by the falling arrow, the initial temperature will be eventually reached

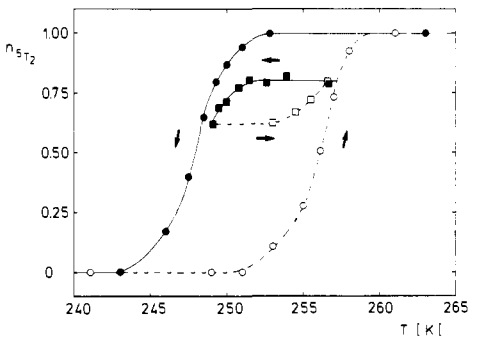

Figure 2. Temperature dependence of the high-spin $^5T_2$ fraction $n_{^5T_2}$ for [Fe(phy)$_2$](ClO$_4$)$_2$ (sample I) on the basis of Mössbauer measurements. Rising arrow indicates increasing temperatures and falling arrow indicates decreasing temperatures ($T_c\uparrow$ = 256.1 K, $T_c\downarrow$ = 248.0 K).

and thus the hysteresis loop is formed. The detailed values of $n_{^5T_2}$ are listed in Table II. A transition temperature T_c may now be defined as that temperature at which $n_{^5T_2}$ = 0.50. It follows that the transition is centered, for increasing temperatures, on $T_c\uparrow$ = 256.1 K, whereas for decreasing temperatures, $T_c\downarrow$ = 248.0 K. The width if the hysteresis loop is therefore 8.1 K.

The scanning curve in Figure 2 has been produced by interrupting the temperature rise in the ascending branch at 256.7 K ($n_{^5T_2}$ = 0.785) and by gradually lowering the temperature to 249.1 K ($n_{^5T_2}$ = 0.619). If the temperature is subsequently increased to 256.6 K ($n_{^5T_2}$ = 0.797), the inner loop of the hysteresis curve is completed. It has been verified that both the scanning curve and the main branches of the hysteresis loop are stable and reproducible as required.

Debye–Waller factors have been determined over the temperature range 120.0–302.0 K from the ^{57}Fe Mössbauer spectra as outlined in the Experimental Section. For ascending temperatures, the overall Debye–Waller factor shows a discontinuity at $T_c\uparrow$ = 256.1 K, the Debye–Waller factor for the $^5T_2$ phase being 42% lower than that for the $^1A_1$ phase; i.e., $f_{^5T_2}$ = 0.116 and $f_{^1A_1}$ = 0.198 at $T_c\uparrow$ = 256.1 K. The temperature dependence of both $f_{^5T_2}$ and $f_{^1A_1}$ may be well reproduced within the high-temperature approximation of the Debye model

$$-\ln f_{(T\geq\Theta/2)} = \frac{3E_0^2}{Mc^2k}\left(\frac{T}{\Theta}\right) \qquad (8)$$

In eq 8, E_0 is the γ-ray energy (E_0 = 14.4 keV), Θ the Debye temperature, and, for simple atomic lattices, M the mass of the absorbing atom. Application of eq 8 to the experimental data produces

$$\Theta_{^5T_2} = 127.3 \text{ K} \qquad \Theta_{^1A_1} = 146.8 \text{ K}$$

if, for the purpose of comparison, M is identified with the mass of the ^{57}Fe atom, M_{Fe} = 57 au.

The magnetism of [Fe(phy)$_2$](ClO$_4$)$_2$ (sample I) has been measured between 353 and 137 K both with decreasing and with increasing temperature. At 353 K, μ_{eff} = 5.19 μ_B is indicative of a high-spin $^5T_2$ ground state, whereas at 137 K μ_{eff} = 0.66 μ_B

Table III. Magnetic Susceptibility χ_m^{corr} [a] and Effective Magnetic Moment μ_{eff} [b] for $[Fe(phy)_2](ClO_4)_2$ (Sample I)[c]

T, K	$10^6\chi_m^{corr}$, cgs/mol	μ_{eff}, μ_B
353	9560	5.19
333	10060	5.18
313	10680	5.17
303	11100	5.19
284	11740	5.16
275	12150	5.17
265	12650	5.18
255	13120	5.17
250	12840	5.07
245	4140	2.85
240	910	1.32
225	410	0.86
215	370	0.80
205	360	0.77
196	350	0.74
166	370	0.70
137	400	0.66
240	530	1.01
245	630	1.11
250	900	1.34
255	9520	4.41
260	12880	5.18
275	12190	5.18

[a] Molecular weight $M = 851.5$; diamagnetic correction is -371×10^{-6} cgs/mol; experimental uncertainty is ±100 cgs/mol. [b] $\mu_{eff} = 2.828(\chi_m^{corr}T)^{1/2}$; experimental uncertainty is ±0.02 μ_B. [c] The values are listed in the order of measurement.

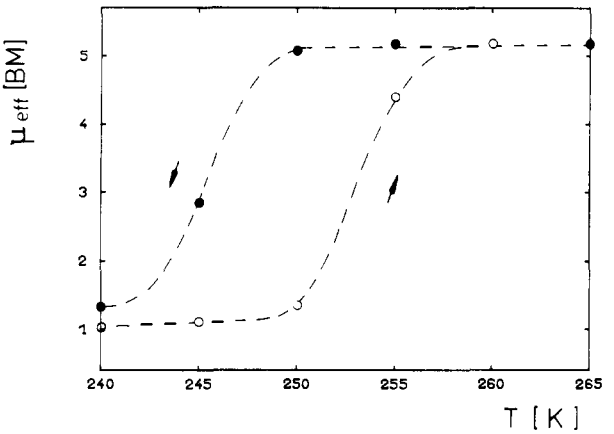

Figure 3. Effective magnetic moment μ_{eff} of $[Fe(phy)_2](ClO_4)_2$ (sample I) as a function of temperature in the region of T_c.

is consistent with a low-spin $^1A_1$ ground state. The detailed magnetic data are listed in Table III; the temperature dependence of μ_{eff} in the region of the transition is illustrated by Figure 3.

The temperature dependence of peak profiles of the X-ray diffraction pattern of $[Fe(phy)_2](ClO_4)_2$ (sample I) was studied between 77 and 300 K as outlined in the Experimental Section. Figure 4 shows the peak profiles for diffraction angles between $\theta = 3.30$ and 5.10° (left diagram) and between $\theta = 7.60$ and 10.0° (right diagram) at the temperatures 249.0, 253.8, and 259.0 K. At low temperatures, i.e., 249.0 K and below, four intense powder peaks are found in the region being monitored and these are assigned to the $^1A_1$ ground state as indicated by the Mössbauer spectra. The peaks remain isolated up to 249.0 K, their position showing only very small changes due to thermal expansion of the lattice. Above 250 K, four additional peaks become visible, their intensity increasing with ascending temperature while a concomitant decrease in the intensity of the $^1A_1$ lines is observed. The four additional peaks are assigned to the $^5T_2$ ground state, again taking the Mössbauer spectra as a reference. Above 257.0 K, the diffraction pattern is characterized by the $^5T_2$ diffraction peaks alone. The values of the diffraction angle θ and the spacing d for the individual powder lines are listed in Table IV. Note that peak profiles were collected in the transition region both within

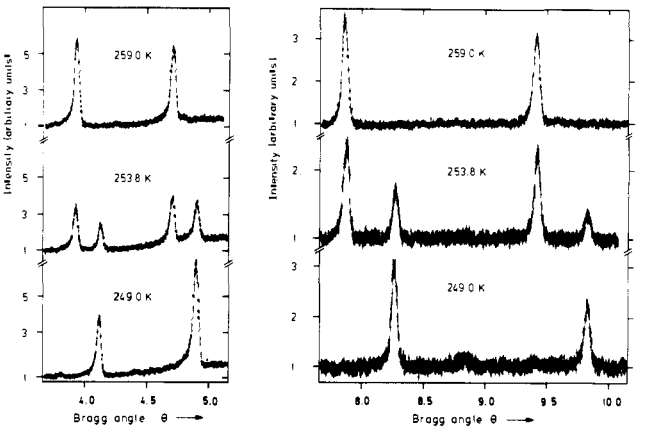

Figure 4. Peak profiles of X-ray powder diffraction for $[Fe(phy)_2](ClO_4)_2$ (sample I) at 249.0, 253.8, and 259.0 K. The measurements were performed for increasing temperatures ($T_c\uparrow$ = 253.1 K). The diagram at the left is for the range $3.15° < \theta < 5.15°$ and the diagram at the right for $7.15° < \theta < 10.15°$.

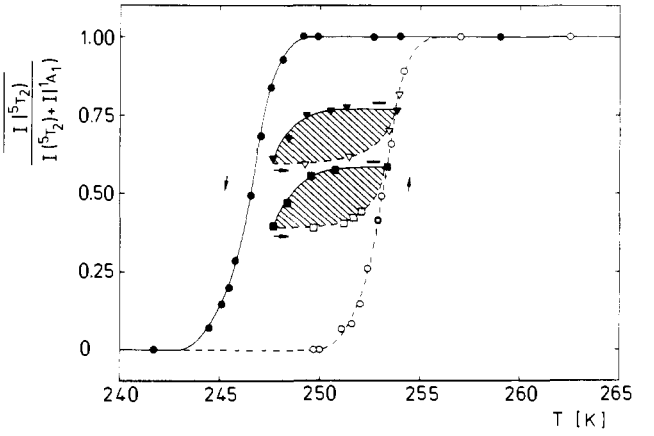

Figure 5. Temperature dependence of the average relative intensity of the $^5T_2$ peak profiles, $I(^5T_2)/[I(^5T_2) + I(^1A_1)]$, for $[Fe(phy)_2](ClO_4)_2$ (sample I). Rising arrow indicates increasing temperatures and falling arrow indicates decreasing temperatures ($T_c\uparrow$ = 253.1 K, $T_c\downarrow$ = 246.5 K).

Table IV. Diffraction Angle θ and Spacing d for Four Characteristic Powder Lines in the $^1A_1$ and $^5T_2$ Phases of $[Fe(phy)_2](ClO_4)_2$ (Sample I) at $T_c\uparrow$ = 253.1 K[a]

line no.	$^1A_1$		$^5T_2$	
	θ, deg	d, Å	θ, deg	d, Å
1	4.12	10.72	3.92	11.27
2	4.90	9.03	4.69	9.42
3	8.28	5.35	7.87	5.63
4	9.84	4.51	9.42	4.71

[a] The experimental uncertainty of θ and d is ±0.02.

1 h and within 20 h at the same temperature, equal relative intensities having been obtained for both measurements. If the temperature is gradually lowered from high temperatures, the high-spin ($^5T_2$) ⇌ low-spin ($^1A_1$) transition takes place at a lower temperature than with increasing temperature. The sample thus shows crystallographic hysteresis effects at the transition.

In order to obtain quantitative data from the analysis of the results of X-ray diffraction measurements, we have plotted the relative intensity of the $^5T_2$ peak profiles, $I(^5T_2)/[I(^5T_2) + I(^1A_1)]$, in Figure 5, as a function of temperature for a complete temperature cycle. In fact, the relative intensity of all four $^5T_2$ lines of Figure 4 has been averaged in order to improve the accuracy of the results. In addition, two scanning curves have been determined for $[Fe(phy)_2](ClO_4)_2$ (sample I), and these have been incorporated into Figure 5. The detailed data are given in Table V. The transition temperatures for the two branches of the

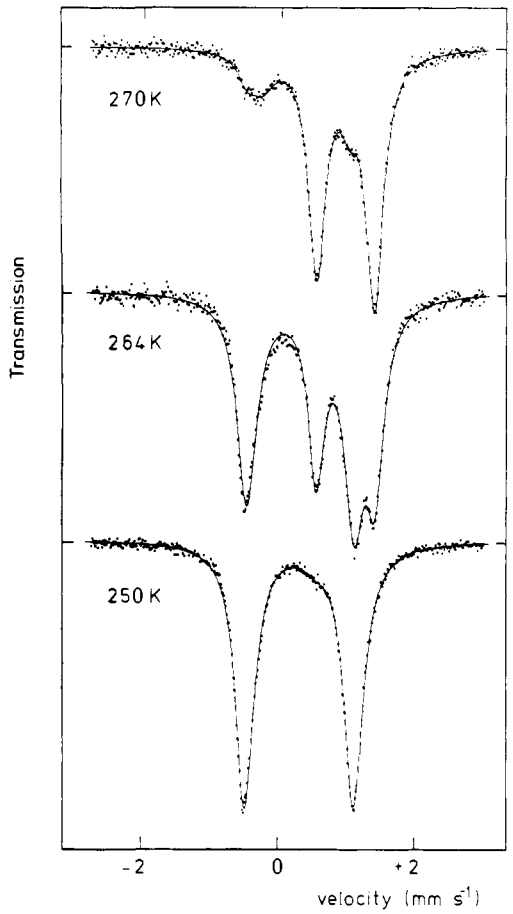

Figure 6. ^{57}Fe Mössbauer effect spectra of [Fe(phy)$_2$](ClO$_4$)$_2$ (sample II), at 250, 264, and 270 K. The measurements were performed for increasing temperatures ($T_c\uparrow$ = 262.8 K).

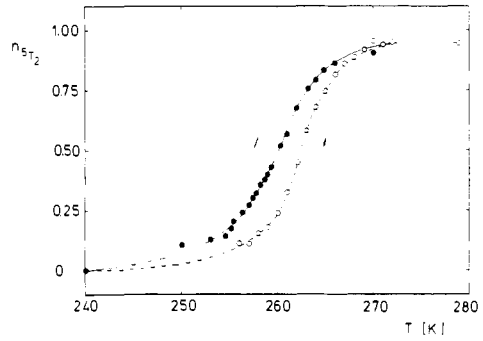

Figure 7. Temperature dependence of the high-spin $^5T_2$ fraction $n_{^5T_2}$ for [Fe(phy)$_2$](ClO$_4$)$_2$ (sample II) on the basis of Mössbauer measurements. Rising arrow indicates increasing temperatures and falling arrow indicates decreasing temperatures ($T_c\uparrow$ = 262.8 K, $T_c\downarrow$ = 260.0 K).

hysteresis loop may be now easily determined as $T_c\uparrow$ = 253.1 K and $T_c\downarrow$ = 246.5 K. The hysteresis loop thus shows a width of 6.6 K.

Sample II. Sample II of [Fe(phy)$_2$](ClO$_4$)$_2$ has been prepared by using iron enriched to >90% with ^{57}Fe. No chemical difference from sample I has been detected.

The ^{57}Fe Mössbauer effect study of [Fe(phy)$_2$](ClO$_4$)$_2$ (sample II) produced values of quadrupole splitting ΔE_Q and isomer shift δ^{IS} for the two ground states, high-spin $^5T_2$ and low-spin $^1A_1$, which are identical within the error of measurement, with the corresponding values of sample I. Thus, at 264.0 K, e.g., the result is $\Delta E_Q(^1A_1)$ = 1.59 ± 0.01 mm s^{-1}, $\delta^{IS}(^1A_1)$ = +0.28 ± 0.01 mm s^{-1}, and $\Delta E_Q(^5T_2)$ = 0.85 ± 0.01 mm s^{-1}, $\delta^{IS}(^5T_2)$ = +0.95 ± 0.01 mm s^{-1}. Mössbauer spectra in the region of $T_c\uparrow$, i.e., at 250, 264, and 270 K, are shown in Figure 6. A detailed Mössbauer effect study of the $^5T_2$ fraction, $n_{^5T_2}$, as a function of temperature (cf. Figure 7) shows, however, that the hysteresis curve for sample II is considerably more narrow than that for sample I. In addition, the transition is less sudden in that it extends over more than 20 K. The transition temperatures are found to be $T_c\uparrow$ = 262.8 K and $T_c\downarrow$ = 260.0 K; the width of the hysteresis loop is 2.8 K. The full data for $n_{^5T_2}$ are listed in Table VI.

At $T_c\uparrow$ = 262.8 K, the Debye-Waller factor for the $^5T_2$ phase is found to be 60% smaller than that for the $^1A_1$ phase; i.e., $f_{^5T_2}$ = 0.071 and $f_{^1A_1}$ = 0.178 at $T_c\uparrow$ = 262.8 K. As before, these measurements have been performed for rising temperatures. Also, the high-temperature approximation of the Debye model is again followed by both $f_{^5T_2}$ and $f_{^1A_1}$ (cf. eq 8), the resulting Debye temperatures being

$$\Theta_{^5T_2} = 116.6 \text{ K} \qquad \Theta_{^1A_1} = 144.2 \text{ K}$$

whereby M_{Fe} = 57 au has been used.

The magnetism of [Fe(phy)$_2$](ClO$_4$)$_2$ (sample II) has been measured between 353 and 128 K, the magnetic moment varying between 5.53 μ_B at 353 K and μ_{eff} = 1.20 μ_B at 128 K. The narrow and extended form of the hysteresis curve (viz., Figure 7) is well reproduced by the temperature dependence of μ_{eff} displayed in Figure 8, the complete data being listed in Table VII.

Similar to sample I, the X-ray powder diffraction of [Fe(phy)$_2$](ClO$_4$)$_2$ (sample II) shows four diffraction lines in the

Table VII. Magnetic Susceptibility χ_m^{corr} [a] and Effective Magnetic Moment μ_{eff} [b] for [Fe(phy)$_2$](ClO$_4$)$_2$ (Sample II)[c]

T, K	$10^6\chi_m^{corr}$, cgs/mol	μ_{eff}, μ_B
299	12380	5.46
128	1400	1.20
147	1320	1.25
166	1320	1.33
186	1400	1.45
206	1400	1.52
225	1490	1.64
245	1920	1.95
265	10060	4.64
275	13490	5.47
270	13320	5.39
265	12720	5.21
260	9210	4.39
255	4060	2.89
250	2340	2.17
245	2090	2.03
240	1830	1.88
245	2090	2.03
250	2430	2.21
255	2860	2.42
260	6290	3.63
265	11440	4.94
270	13410	5.40
275	13320	5.44
308	12294	5.53
323	11690	5.52
338	11090	5.50
353	10750	5.53

[a] Molecular weight M = 851.5; diamagnetic correction is −371 × 10^{-6} cgs/mol; experimental uncertainty is ±100 cgs/mol. [b] $\mu_{eff} = 2.828(\chi_m^{corr}T)^{1/2}$; experimental uncertainty is ±0.02 μ_B. [c] The values are listed in the order of measurement.

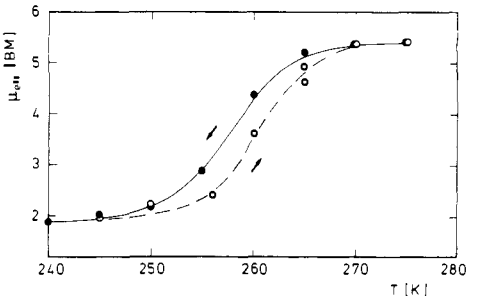

Figure 8. Effective magnetic moment μ_{eff} of [Fe(phy)$_2$](ClO$_4$)$_2$ (sample II) as a function of temperature in the region of T_c.

Table VIII. Diffraction Angle θ and Spacing d for Four Characteristic Powder Lines in the $^1A_1$ and $^5T_2$ Phases of $[Fe(phy)_2](ClO_4)_2$ (Sample II) at $T_c\uparrow = 261.1$ K[a]

line no.	$^1A_1$		$^5T_2$	
	θ, deg	d, Å	θ, deg	d, Å
1	4.09	10.81	3.90	11.33
2	4.86	9.09	4.67	9.46
3	8.24	5.38	7.87	5.63
4	9.81	4.52	9.41	4.71

[a] The experimental uncertainty of θ and d is ±0.02.

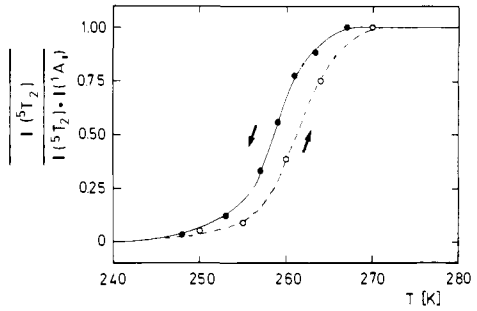

Figure 9. Temperature dependence of the average relative intensity of the $^5T_2$ peak profiles, $I(^5T_2)/[I(^5T_2) + I(^1A_1)]$, for $[Fe(phy)_2](ClO_4)_2$ (sample II). Rising arrow indicates increasing temperatures and falling arrow indicates decreasing temperatures ($T_c\uparrow = 261.1$ K, $T_c\downarrow = 258.0$ K).

relevant region which are stable at low temperatures and which transform into four different lines at high temperatures (cf. Figure 3 of Irler et al.[14]). The positions of the individual lines are listed in Table VIII. They are very close to those found for sample I; cf. Table IV. It may be concluded that, on a crystallographic basis, both samples of $[Fe(phy)_2](ClO_4)_2$ are largely the same. Significant differences arise, however, if the relative intensity of the $^5T_2$ peak profiles, $I(^5T_2)/[I(^5T_2) + I(^1A_1)]$, is considered as a function of temperature as shown in Figure 9. Again the average values of the four peak profiles were employed, the detailed data being listed in Table IX. The transition temperatures for the two branches of the hysteresis loop were found to be $T_c\uparrow = 261.1$ K, $T_c\downarrow = 258.0$ K, the width of the loop thereby amounting to 3.1 K.

Recrystallized Sample II. Sample II of $[Fe(phy)_2](ClO_4)_2$ has been carefully reinvestigated after a further recrystallization.

The ^{57}Fe Mössbauer effect parameters ΔE_Q and δ^{IS} for the two ground states, $^5T_2$ and $^1A_1$, were found to be identical with those of the sample before recrystallization. However, the hysteresis curve based on the Mössbauer $^5T_2$ fraction shows significant differences with respect to that of sample II before recrystallization (cf. Figure 10). In particular, the transition temperatures, $T_c\uparrow = 251.5$ K and $T_c\downarrow = 241.6$ K, and the width of the hysteresis loop $\Delta T_c = 9.9$ K as well as the steep character of the curves are more reminiscent of the results for sample I. It should be noted that, compared to sample I, the transition is shifted to lower temperature, viz., 4.6 K for the ascending and 6.4 K for the descending boundary curve.

Debye–Waller factors were also determined, the results being $f_{^5T_2} = 0.096$ and $f_{^1A_1} = 0.164$ at $T_c\uparrow = 251.5$ K. Consequently, $f_{^5T_2}$ is 41% lower than $f_{^1A_1}$, again close to the results for sample I. From the high-temperature approximation of the Debye model, one obtains moreover

$$\Theta_{^5T_2} = 120.9 \text{ K} \qquad \Theta_{^1A_1} = 137.6 \text{ K}$$

The effective magnetic moment of the recrystallized sample II of $[Fe(phy)_2](ClO_4)_2$ shows a variation between $\mu_{eff} = 5.34\ \mu_B$ at 303.0 K and $\mu_{eff} = 1.09\ \mu_B$ at 118.0 K, the form of the hysteresis curve being closely similar to that of Figure 10. Finally it was verified, by measurements at a number of selected temperatures, that the recrystallized sample II shows the same X-ray powder diffraction lines and the corresponding changes with temperature as the samples described above.

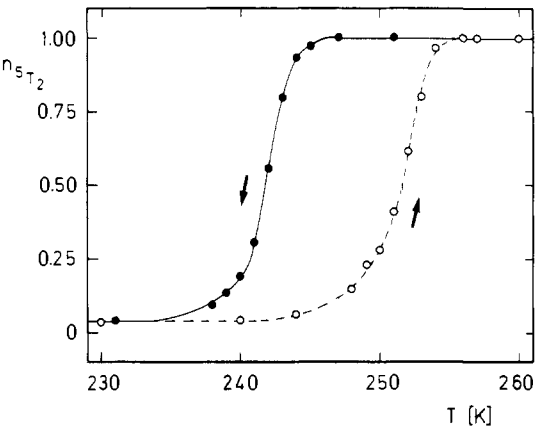

Figure 10. Temperature dependence of the high-spin $^5T_2$ fraction $n_{^5T_2}$ for $[Fe(phy)_2](ClO_4)_2$ (sample II) after recrystallization, on the basis of Mössbauer measurements. Rising arrow indicates increasing temperatures and falling arrow indicates decreasing temperatures ($T_c\uparrow = 251.5$ K, $T_c\downarrow = 241.6$ K).

Discussion

Following the conventional thermodynamic classification, a transition of first order is characterized by definition,[20,21] by a discontinuous change of energy, i.e., a latent heat, and by discontinuities in volume and in lattice parameters. As a consequence, the transition takes place sharply at a particular temperature. In the case of $[Fe(phy)_2](ClO_4)_2$, samples I and II, a discontinuous change of lattice parameters and thus volume may be inferred from the study of X-ray diffraction and the Debye–Waller factor. It has been shown elsewhere[13,22] that the almost discontinuous high-spin ($^5T_2$) ⇌ low-spin ($^1A_1$) transition in $[Fe(4,7\text{-}(CH_3)_2phen)_2(NCS)_2]$ and in $[Fe(bt)_2(NCS)_2]$ where phen = 1,10-phenanthroline and bt = 2,2′-bi-2-thiazoline may be rationalized in terms of a Bragg and Williams type model.[23] This type of interpretation is applicable to $[Fe(phy)_2](ClO_4)_2$ as well and requires a latent heat and a change in entropy. Therefore, the observed high-spin ($^5T_2$) ⇌ low-spin ($^1A_1$) transition in *solid* $[Fe(phy)_2](ClO_4)_2$ may be considered as a transition of *first order*.

The observation of hysteresis effects is likewise restricted to phase transitions of first order. Hysteresis curves have been studied for both samples I and II of $[Fe(phy)_2](ClO_4)_2$ by three different methods, viz., ^{57}Fe Mössbauer effect, peak profiles of X-ray diffraction, and magnetism. The agreement between the results of these measurements on the same sample, e.g., sample I, is most gratifying; cf. $T_c\uparrow = 256.1$ K, $T_c\downarrow = 248.0$ K, and $T_c\uparrow = 253.1$ K, $T_c\downarrow = 246.5$ K for the Mössbauer effect and X-ray diffraction measurements, respectively. The differences between corresponding values of T_c have to be attributed to the different methods of measurement. It proved to be extremely difficult to achieve an identical calibration over the range 80–300 K for the different temperature sensors used.

Of particular interest is the agreement between the temperature functions and thus the hysteresis curves of the crystallographic (viz., eq 7) and the molecular or iron atom based (i.e., from the ^{57}Fe Mössbauer effect) high-spin fractions $n_{^5T_2}$ (cf. Figures 2 and 5 for sample I and Figures 7 and 9 for sample II). The close correspondence demonstrates that, in the solid compound, the electronic state of the molecules changes at the $^5T_2 \rightleftharpoons {}^1A_1$ transition *simultaneously* with the crystallographic properties of the lattice.

Hysteresis effects may be particularly well understood on the basis of a model developed by Everett.[24-26] According to this

(20) A. Münster in "Handbook of Physics", Vol. III/2, S. Flügge Ed., Springer-Verlag, West Berlin, 1959, p 373.
(21) P. Ehrenfest, *Commun. Kamerlingh Onnes Lab. Univ. Leiden Suppl., No. 75b* (1933).
(22) E. König and G. Ritter, *Solid State Commun.*, **18**, 279 (1976).
(23) C. P. Slichter and H. G. Drickamer, *J. Chem. Phys.*, **56**, 2142 (1972).
(24) D. H. Everett and W. I. Whitton, *Trans. Faraday Soc.*, **48**, 749 (1952).
(25) D. H. Everett and F. W. Smith, *Trans. Faraday Soc.*, **50**, 187 (1954).

model, a sample showing a collective phase transition may be considered as built up of macroscopic domains, each domain i showing a sharp transition temperature $T_{c,i}\uparrow$ for rising and similarly $T_{c,i}\downarrow$ for falling temperature.[27] The quantity $\Delta_i = T_{c,i}\uparrow - T_{c,i}\downarrow$ is different for individual domains since, if the values of Δ_i were the same for all i, the temperature could be varied within the boundaries of the hysteresis curve without changing the high-spin fraction, $n_{^5T_2}$. It has been shown above, however, that scanning curves may be obtained (cf. Figures 2 and 5). Everett and Smith[25] derived a number of theorems which apply to the scanning curves within the domain model. The present results are clearly seen to conform to their general theorems 2 and 3. The key theorem (i.e., theorem 4 of ref 25) states that, for independent domains, the shapes and areas of scanning curves between the same two values of temperature should be equal. Figure 5 shows two scanning curves which have been determined on $[Fe(phy)_2](ClO_4)_2$ (sample I) between practically identical temperatures. It has been found that the areas bound by the two curves are equal to within 3%. The results are therefore consistent with the assumption of domain formation by both $^5T_2$ and $^1A_1$ molecules, whereby any interaction between domains should be negligible.

The width of X-ray powder diffraction lines shows a well-known dependence on the mean size of the crystals.[28] In the present study, all observed diffraction lines show the minimum line width which is achievable under the given instrumental conditions. It follows that the observed diffraction lines are produced by domains of magnitude ≥5000 Å. The powder particles in the samples used in this work are approximately of this magnitude. Consequently, it may be assumed that, except for dislocations in larger grains, the domains of the Everett model are in effect the actual particles of the samples.

It is evident that the volume difference between the $^1A_1$ and $^5T_2$ ground states of the $[Fe(phy)_2](ClO_4)_2$ molecule will play an important role in the mechanism of the cooperative high-spin ($^5T_2$) ⇌ low-spin ($^1A_1$) transition within an individual domain. According to investigations by Beattie et al.[9,10] $V_M(^5T_2)$ is always greater than $V_M(^1A_1)$ with ΔV_M varying between about 10 and 22 $cm^3\ mol^{-1}$. The $^5T_2 \rightleftharpoons {}^1A_1$ phase transition in the solid compound may be qualitatively described as follows. If, in a domain of $^1A_1$ molecules, the temperature is increased to T_c, a limited number of molecules may show a conversion $^1A_1 \rightarrow {}^5T_2$. The larger $^5T_2$ molecules will be subject to pressure by the surrounding $^1A_1$ lattice. As a consequence, the domain will show a collective phase transition to the energetically more favorable $^5T_2$ state only at a higher temperature $T > T_c$ ("superheating"). Conversely, the $^5T_2$ lattice will exert a tension on isolated $^1A_1$ molecules which may form on lowering of temperature to T_c. In this case, the domain will show a phase transition $^5T_2 \rightarrow {}^1A_1$ only at a lower temperature $T < T_c$ ("supercooling"). The transformation in a particular domain will thus be inhibited in both directions by the lattice and this inhibition will produce the hysteresis effects observed. Indeed a correlation between the width of the hysteresis curve and ΔV_M has been found for phase transitions in certain ammonium salts.[29] The larger ΔV_M, the larger the hysteresis width.

It is well known that phase transitions of first order may be "smeared out" to some extent, the origin of this effect usually being local nonuniformities and stresses due to various inner defects or to grain boundaries between crystals. In the present study, sample II of $[Fe(phy)_2](ClO_4)_2$ shows a hysteresis curve which extends over a significantly larger temperature interval than for sample I. Despite the "continuous" character of the transition, the presence of hysteresis and other characteristic properties show that a phase transition similar to that in sample I is present. Thus the first-order character of the transition in sample II is diminished due to a wider distribution of transition temperatures for the domains which is caused by impurities and/or defects of the solid. This conclusion finds additional support in the fact that after recrystallization, sample II shows hysteresis properties similar to those of sample I. If the volume difference ΔV_M is indeed the determining quantity for phase transitions of the type considered, hysteresis curves showing steep boundaries will be the only ones which will provide physically valuable information.

The almost discontinuous high-spin ($^5T_2$) ⇌ low-spin ($^1A_1$) transitions in two other iron(II) complexes, *i.e.*, $[Fe(bt)_2(NCS)_2]$ where bt = 2,2′-bi-2-thiazoline,[13] and $[Fe(4,7\text{-}(CH_3)_2phen)_2(NCS)_2]$[30] have been studied with results similar to those reported here. It is not unlikely that the present conclusions are of general applicability to abrupt spin transitions in solids. The mechanism responsible for discontinuous high-spin ($^5T_2$) ⇌ low-spin ($^1A_1$) transitions in solid iron(II) compounds is thus significantly different from that encountered for spin equilibria in the solutions of iron(II) complexes.[9,11]

Acknowledgments. The authors appreciate financial support by the Deutsche Forschungsgemeinschaft and the Fonds der Chemischen Industrie.

Note Added in Proof. Since submission of the manuscript, the first multiple temperature X-ray structure analysis of a high-spin ($^5T_2$) ⇌ low-spin ($^1A_1$) transition was reported.[31] Of particular interest is the crystallographic resolution of the two-spin isomers of the studied complex, $[Fe(2\text{-pic})_3]Cl_2 \cdot CH_3OH$ where 2-pic = 2-picolylamine.

Supplementary Material Available: (1) the high-spin fraction $n_{^5T_2}$ for the hysteresis loop of $[Fe(phy)_2](ClO_4)_2$ (sample I) from Table II; (2) the relative intensity of the $^5T_2$ peak profiles, $I_{rel} = I(^5T_2)/[I(^5T_2) + I(^1A_1)]$, for $[Fe(phy)_2](ClO_4)_2$ (sample I) from Table V; (3) the high-spin fraction $n_{^5T_2}$ for the main branches of the hysteresis loop of $[Fe(phy)_2](ClO_4)_2$ (sample II) from Table VI; (4) the relative intensity of the $^5T_2$ peak profiles, $I_{rel} = I(^5T_2)/[I(^5T_2) + I(^1A_1)]$, for $[Fe(phy)_2](ClO_4)_2$ (sample II) from Table IX (7 pages). Ordering information is given on any current masthead page.

(26) D. H. Everett, *Trans. Faraday Soc.*, **50**, 1077 (1954); **51**, 1551 (1955).
(27) The phase transition within each individual domain may be reasonably well described in terms of a Bragg and Williams type model.[23]
(28) H. P. Klug and L. E. Alexander, "X-Ray Diffraction Procedures for Polycrystalline and Amorphous Materials", Wiley, New York, 1954.
(29) A. R. Ubbelohde, *J. Chim. Phys. Phys.-Chim. Biol.*, **62**, 33 (1966).
(30) E. König, G. Ritter, and W. Irler, *Chem. Phys. Lett.*, **66**, 336 (1979).
(31) B. A. Katz and C. E. Strouse, *J. Am. Chem. Soc.*, **101**, 6214 (1979).